Heterogeneous Uptake of Gaseous Nitric Acid on Dolomite ($CaMg(CO_3)_2$) and Calcite ($CaCO_3$) Particles: A Knudsen Cell Study Using Multiple, Single, and Fractional Particle Layers

Elizabeth R. Johnson,[†] Joanna Sciegienka,[‡] Sofia Carlos-Cuellar,[†] and Vicki H. Grassian*[,†,‡]

Department of Chemistry and Environmental Sciences Program, University of Iowa, Iowa City, Iowa 52242

Received: March 30, 2005; In Final Form: May 20, 2005

In this study, the heterogeneous uptake of gaseous nitric acid on dolomite, $CaMg(CO_3)_2$, and calcite, $CaCO_3$, particles under dry conditions at 296 K was investigated. A Knudsen cell reactor was used to measure heterogeneous uptake coefficients for these reactions. Several different experiments were performed including those on many, single, and fractional layers of particles. For experiments using multiple particle layers, the Knudsen cell data were modeled to take into account gas diffusion into the underlying layers of the sample. From this analysis, initial heterogeneous uptake coefficients, $\gamma_{o,t}$, were determined to be $(5 \pm 2) \times 10^{-4}$ and $(2 \pm 1) \times 10^{-3}$, for dolomite and calcite, respectively, at a nitric acid concentration of 6.5×10^{10} molecules cm^{-3}. For experiments that employed single or fractional particle layers, the initial heterogeneous uptake coefficient was analyzed using a recent method described in the literature. Values of the initial heterogeneous uptake coefficient using this analysis were in agreement with the above analysis and determined to be $(7 \pm 4) \times 10^{-4}$ and $(2 \pm 0.4) \times 10^{-3}$ for $CaMg(CO_3)_2$ and $CaCO_3$, respectively. In addition, these results are compared to previous literature values.

Introduction

It has been estimated that 3000−5000 Tg of particulates are emitted into the troposphere annually.[1] Approximately 1000−3000 Tg of that amount is made up of mineral dust aerosol.[2] Other types of particulates that are also present in the troposphere include sea salt, soot, organics, and sulfate aerosols. These particulates provide a large amount of surface area that can facilitate heterogeneous chemistry. Mineral dust in the troposphere often comes in the form of windblown soils and is composed largely of metal oxides, clays, and carbonates.[3,4] As arid and semiarid regions of the globe expand, the amount of mineral dust emitted into the troposphere may increase significantly.

Understanding heterogeneous reactions that occur on the surface of aerosol particles will lead to a better understanding of the fate and transport of molecules in the troposphere as well as air quality and air pollution. One of the major components of air pollution is nitrogen-containing species, such as NO_x (NO_2 + NO) and HNO_3. Heterogeneous reactions that affect NO_x and HNO_3 concentrations are expected have an important impact on the overall chemical balance of the troposphere through coupled processes. With the prediction that the amount of mineral dust aerosol emitted into the troposphere will increase in the years ahead, it is important to gain an understanding of the heterogeneous reactions that may occur on the surface of these particles.

Several modeling studies have investigated the potential impact of mineral dust interactions with trace atmospheric gases. These modeling studies have concluded that mineral dust aerosol will substantially alter the chemical balance of the troposphere by specifically lowering HNO_3 concentrations.[5−9] Song and Carmichael[10] as well as Tabazadeh et al.[11] have suggested that carbonate minerals such as $CaCO_3$ may be particularly effective minerals in the uptake of HNO_3. The stoichiometric bulk reaction for this heterogeneous process can be written as

$$CaCO_3(s) + 2HNO_3(g) \rightarrow Ca(NO_3)_2(s) + CO_2(g) + H_2O(g) \quad (1)$$

When available, atmospheric chemistry models use input from laboratory investigations of the kinetics of these reactions. One current problem, as recently discussed by Bian and Zender,[8] is that there are discrepancies in the values of heterogeneous reaction rates that span orders of magnitude from different laboratory studies. An important reason for the discrepancy in the reported reaction rates is the difference in the amount of surface area that is used to determine the heterogeneous uptake coefficient. Often experiments are done on powdered samples that consist of multiple particle layers instead of suspended isolated particles. For powdered samples, the reactant gas can potentially diffuse through the particle layers and access a surface area that is greater than the geometric area of the sample holder, which is often used to calculate initial uptake coefficients. It has been suggested that the geometric surface area of the sample holder is a good approximation of surface area when the reaction is very fast, i.e., uptake coefficients close to 1, and the gas is taken up before it can diffuse into lower layers. However, when the heterogeneous reaction rate is slow, the use of the geometric area of the sample holder is not a good measure of the available surface area and there is a contribution of underlying layers due to the diffusion that must be taken into account.[12,13]

Although there is general agreement in calculating reaction rates and heterogeneous uptake coefficients reactions involving O_3 on mineral dust[14−18] and N_2O_5 on salt,[19−23] there has been disagreement concerning the reaction of nitric acid on salt[21,24,25] and mineral dust particles.[12,26−29] In the case of NaCl particles,

* To whom correspondence should be addressed.
[†] Department of Chemistry.
[‡] Environmental Sciences Program.

10.1021/jp0516285 CCC: $30.25
Published on Web 07/15/2005

much of the earlier literature used the geometric area of the sample holder to calculate heterogeneous uptake coefficients. However recently, several groups have reported mass-dependent behavior, correlated to an increase in surface area, of the observed uptake coefficient on salt surfaces. Hoffman et al. report an observed surface area dependence for HNO_3 uptake on NaCl. To determine accurate values of the uptake coefficient, Hoffman et al. developed a method and model whereby fractional layers of particles were used to calculate heterogeneous reaction rates. The use of single or fractional layers eliminates any issues related to gas diffusion into the underlying layers.[30]

Zangmeister and Pemberton recently reported a correction to their previously published value for the uptake coefficient for the reaction of HNO_3 on NaCl. By correcting for the BET surface area, a value of the reaction probability decreased by several orders of magnitude, the uptake coefficient fell within the same range as other published values for this reaction.[31,32] The article by Hoffman provides a more detailed discussion of the literature regarding the heterogeneous uptake of nitric acid on NaCl particles.

In the case of mineral dust particles, Grassian and co-workers have used both the pore diffusion model developed and discussed by Keyser, Moore, and Leu for atmospheric reactions[33] to analyze their data for nitric acid uptake on laboratory surrogates for mineral dust aerosol[28,29,34] and the linear mass dependent regime of the uptake coefficient over a smaller range of powder thicknesses. Both of these methods rely on the BET surface area of the powder to calculate a heterogeneous uptake coefficient. In particular, Underwood et al. have observed a linear mass dependence for the initial uptake coefficient for HNO_3 on several mineral oxides such as α-Al_2O_3, α-Fe_2O_3, and SiO_2, as well as authentic Gobi dust and Saharan sand. Goodman et al. used the pore diffusion model to determine the heterogeneous uptake coefficient of nitric acid on $CaCO_3$. These studies all strongly suggest that the use of the geometric surface area of the sample holder in the calculation of γ does not account for all of the available reactive surface area.

In the work of Hanisch and Crowley, there was no observation of the surface area dependence of the heterogeneous uptake coefficient of nitric acid on laboratory surrogates for mineral dust aerosol.[26,27] One of the main conclusions drawn from this study is that no significant role for internal surfaces below the external surface is evident and that the geometric area could be used in the calculation of the heterogeneous uptake coefficient, which is in direct contrast to the conclusions made by Grassian and co-workers.[12,28,29] It was also suggested by Hanisch and Crowley that discrepancies between values in the literature arise in part from correction factors to account for diffusion into the bulk of the samples, errors from calculating uptake coefficients due to competitive uptake on surfaces other than the sample and determining uptake coefficients at different nitric acid pressures. In addition, it was concluded that the uptake of nitric acid onto mineral dust and clay components is quite high with a value near 0.1.

Very recently, Knudsen cell results by Frinak et al. also report a layer thickness dependence in the uptake of nitric acid on γ-Fe_2O_3.[30,35] In this study, the surface area of the iron oxide particles was measured in situ using water as the adsorbent molecule. Both infrared spectroscopy and mass spectrometry were used to calibrate the amount of water that adsorbed on the iron oxide particles and to determine an in situ specific BET surface area from these different measurements. An important conclusion from the study by Frinak et al. is that underlying surface layers must be taken into account in determining the initial heterogeneous uptake coefficient for nitric acid on γ-Fe_2O_3

Because heterogeneous reactions of mineral dust with HNO_3 may be an important removal process for HNO_3 from the gas phase that can, through coupled processes, influence other important trace atmospheric gases such as ozone, it is essential to have accurate rates for these heterogeneous reactions. Besides the modeling work of Song and Carmichael[10] and Tabazadeh,[11] recent laboratory studies have shown that carbonate particles seem to be a particularly important component of mineral dust aerosol with respect to its reactivity with nitric acid.[36] The purpose of the current study is to reexamine the uptake of HNO_3 on calcite and dolomite using multiple, single, and fractional layers of particles. Uncorrected uptake coefficients are presented to show the dependence that is observed with the use of geometric area. Corrected uptake coefficients are determined from both analysis of the mass dependence and the application of the pore diffusion model for samples that contain multiple layer of particles and the application of the model described by Hoffmann et al. for samples consisting of less than one particle layer.[30] The results from experiments described here should help better quantify the heterogeneous uptake of nitric acid on mineral dust aerosol, at least under dry conditions.

Experimental Methods

Heterogeneous uptake coefficients were measured using two different Knudsen cell reactors that differ in volume by a factor of 15. Both Knudsen cell reactors have been described previously and schematics of these are shown in Figure 1.[12,34,37] Each reactor consists of a chamber with an isolated sample compartment and a small escape aperture through which reactant and product gases can escape and be detected by a quadrupole mass spectrometer. In the Knudsen flow regime, the pressures used are low enough to ensure that the mean free path of the molecules exceeds the dimensions of the cell. The diameter of the escape aperture must be a factor of 10 smaller than the mean free path to ensure molecular flow.[38] This eliminates boundary layer effects and also minimizes gas-phase collisions, which simplifies analysis of the data.

The large volume Knudsen cell reactor ($\sim$1500 cm^3) could accommodate multiple samples holders as shown in Figure 1. The larger volume Knudsen cell reactor consists of a stainless steel reducing cross that has four individual sample holders, which are attached to a platform. Four linear translators are connected to Teflon-coated aluminum disks, serving as covers for the individual samples. All interior surfaces that may be exposed to reactant gases are also Teflon-coated. Viton O-rings provide a seal between the sample holders and the lids. For multilayer experiments, the individual sample holders used are made from stainless steel and have a geometric area of 5.07 cm^2 and a volume of about 2.5 cm^3. Because the total volume of the chamber is close to 1500 cm^3, no corrections are needed to account for the volume change when the sample compartment is opened. This reactor was used for the majority of dolomite experiments that involved multiple, single, and fractional layers of particles. A few experiments on dolomite were carried out in the single sample reactor.

For all fractional layer experiments on dolomite and calcite, the larger volume Knudsen cell reactor was also used to hold a newly designed sample holder and lid with a geometric area of 58.5 cm^2, over 10 times greater than the sample holder used in the multiple layer experiments. The larger sample holder allows for a greater sample loading, providing more surface area and

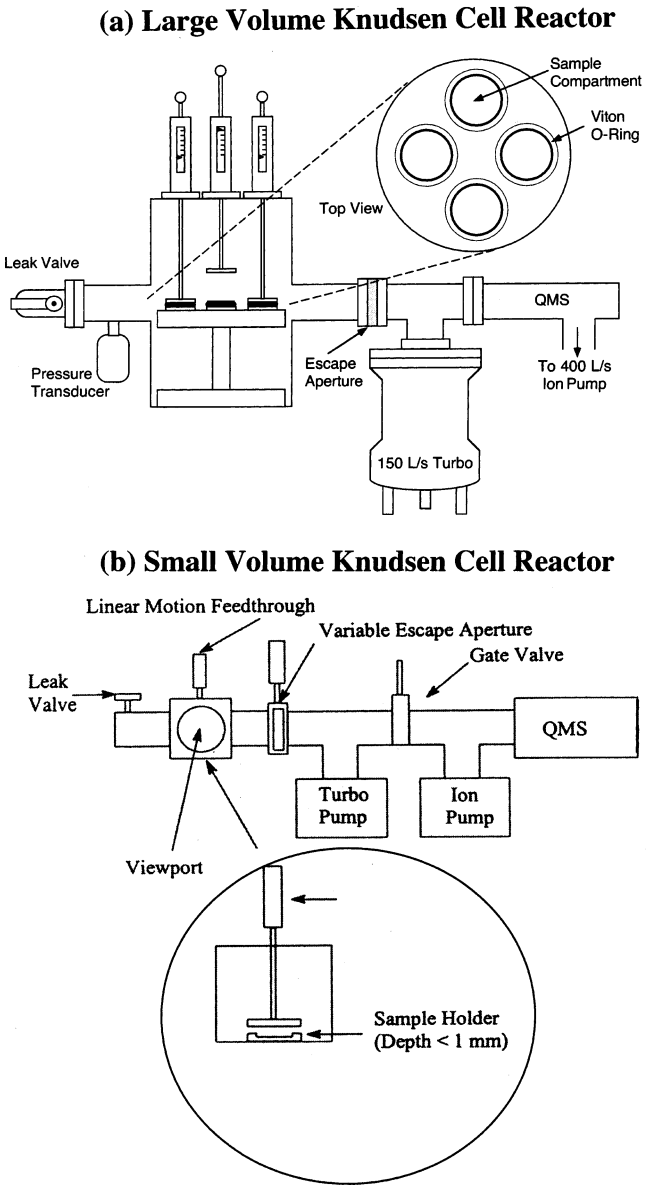

Figure 1. Knudsen cell reactors used in this study are shown above: (a) large volume (~1500 cm^3) system that can accommodate multiple sample holders each with geometric area of 5.07 cm^2 or a large sample holder with a geometric area of 58.5 cm^2 and (b) small volume (~100 cm^3) system with a single sample holder with geometric area of 5.34 cm^2.

thus a significant increase in the signal-to-noise ratio in these experiments involving small total surface area. Because HNO_3 is very reactive with stainless steel, each sample holder, both the large one as well as the smaller ones used in the large volume reactor, was coated with halocarbon wax (Series 1500, Halocarbon Products Corp.), which is inert to nitric acid, as shown in Figure 2. Powdered samples of carbonates were then spread evenly onto the wax surface. Large multilayer samples were lightly packed down to ensure an even distribution of particles across the sample holder.

The large volume Knudsen cell reactor is coupled to a quadrupole mass spectrometer (UTI, DetecTorr II) to allow for detection and monitoring of the reactant gas as well as possible products. The mass spectrometer is equipped with a 400 L/s ion pump and an ion gauge (both from Varian). The area between the Knudsen cell and the mass spectrometer was evacuated with a 150 L/s turbomolecular pump (Leybold TMP/

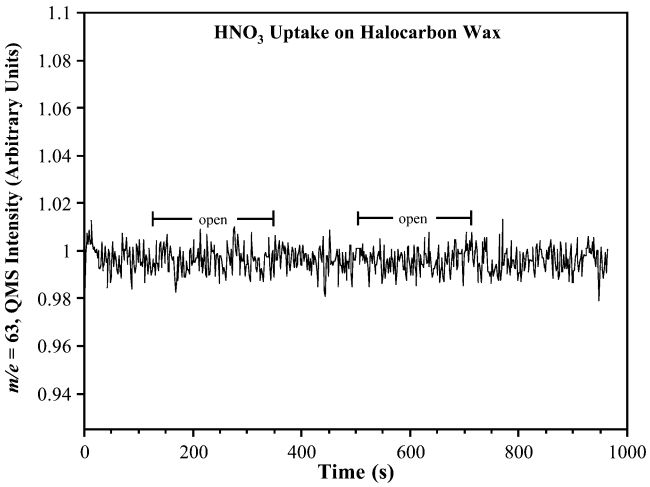

Figure 2. QMS intensity ($m/e = 63$) plotted as a function of time for HNO_3 uptake on halocarbon wax. The sample holder coated with halocarbon wax is exposed to gaseous nitric acid vapor during the times the sample holder lid is open as indicated above. No nitric acid uptake is seen on the halocarbon wax when the sample holder lid is open.

NT-150). Along with the nitric acid parent ion, HNO_3^+ ($m/e = 63$), other mass channels monitored in these experiments include NO_2^+ ($m/e = 46$), an important fragment of HNO_3, along with H_2O^+ ($m/e = 18$) and CO_2^+ ($m/e = 44$). Both H_2O and CO_2 are expected as products in the bulk reaction of nitric acid with carbonate minerals, as shown in eq 1.

Calcite experiments involving multiple layers were mainly conducted in the small volume Knudsen cell reactor. This reactor consists of a stainless steel cube with a volume of 100 cm^3. A single stainless steel sample holder (geometric area of 5.34 cm^2) is covered with a Teflon-coated flange connected to a linear translator. The sample holder is again coated with halocarbon wax. This Knudsen cell reactor is also coupled to a quadrupole mass spectrometer (UTI-100C and UTI DetecTorr II) through a gate valve. The QMS is evacuated with a 150 L/s ion pump (Varian). For experiments in both reactors, the nitric acid was allowed to flow through the reactor prior to data collection until a steady flow was obtained. This was done to passivate the chamber. The gaseous HNO_3 was introduced to the reactor through a leak valve and tuned to a desired pressure as measured with an absolute pressure transducer (MKS 690A.1 TRC, range 1×10^{-6} to 0.1 Torr).

Powdered dolomite samples were obtained by crushing single-crystal dolomite (Alfa Aesar). SEM images of the dolomite sample, shown in Figure 3, were used to characterize the particle shape and size. Dolomite particles were found to have irregular shapes, with a distribution of sizes ranging from 1 to 200 μm. The BET surface area of the crushed powder was measured using a multipoint BET analysis (Quantachrome Nova 1200) and found to be 0.6 $m^2\ g^{-1}$. Two different powders were used as received for calcite samples (Alfa Aesar). SEM images displayed in Figure 4 show that the calcite particles have a somewhat cubic shape and a tendency to form aggregates. Particle sizes for the two calcite samples ranged from 0.2 to 10 μm, with BET surface areas of 0.2 and 1.4 $m^2\ g^{-1}$. Multilayer experiments were conducted using both samples, whereas for fractional layer experiments the 1.4 $m^2\ g^{-1}$ sample was used. Dry gaseous nitric acid was taken from the vapor of a 1:3 by volume solution of concentrated HNO_3 (Fisher Scientific) and H_2SO_4 (Fisher Scientific), purified by several freeze−pump−thaw cycles.

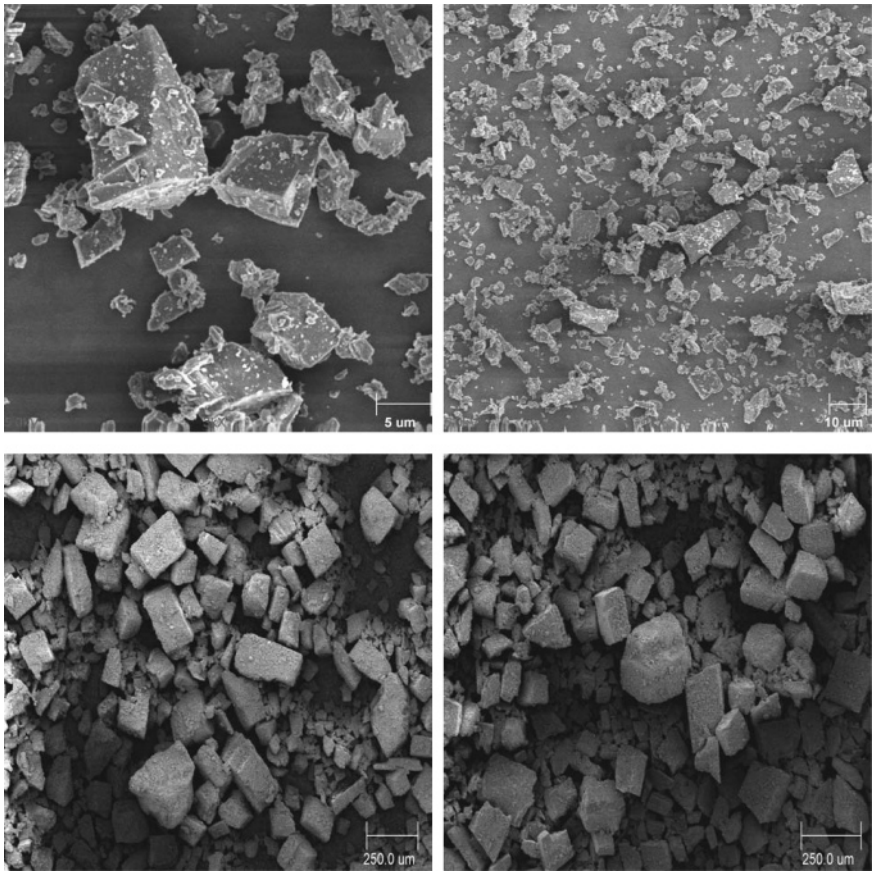

Figure 3. SEM images of dolomite on halocarbon wax. The top two images were used to determine an average particle size and average particle spacing for fractional layer experiments. See text for further details.

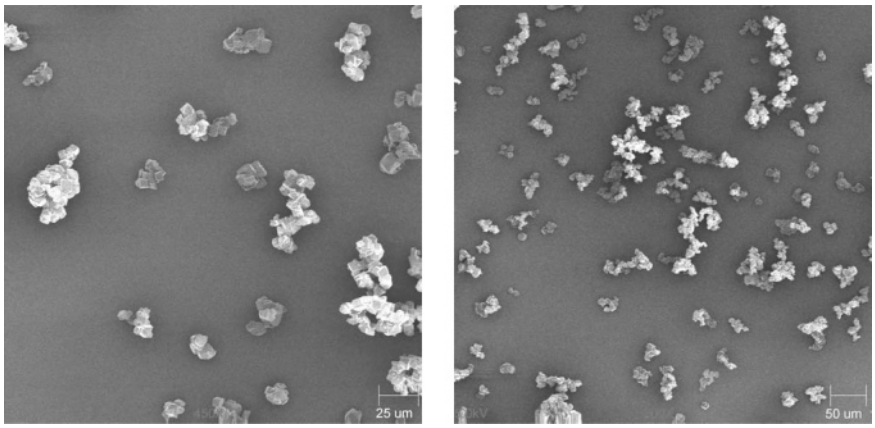

Figure 4. SEM images of calcite on halocarbon wax. The images were used to determine an average particle size and average particle spacing for fractional layer experiments. See text for further details.

Results

Knudsen Cell Reactor Results for Nitric Acid Uptake on Multiple Layers of Dolomite and Calcite Particles. Representative Knudsen cell data for the uptake of HNO_3 on dolomite and calcite particles using samples that contained multiple layers of particles are shown in Figures 5 and 6. A heterogeneous uptake coefficient, γ, can be calculated using the Knudsen cell equation derived for steady-state uptake,

$$\gamma = \frac{A_h}{A_s}\left(\frac{I_0 - I}{I}\right) = \gamma_{obs} \qquad (2)$$

where A_h is the area of the escape aperture, A_s is the geometric area of the sample holder, and I_0 and I are mass spectral intensities that are measured with the sample covered and exposed, respectively. This value of the uptake coefficient is referred to as the observed uptake coefficient, γ_{obs}.

Figure 5a shows Knudsen cell data for the reaction of HNO_3 on dolomite for several samples that differ by the total mass in the sample holder. The nitric acid concentration used in these experiments was 6.5×10^{10} molecules cm^{-3} (corresponding to 2 μTorr). The data displayed in this figure are the result of several experiments for which the QMS intensity curves have been normalized and displaced relative to one another with respect to time. Dolomite is seen to take up HNO_3. The observed uptake coefficient decreases to zero as the surface becomes saturated with adsorbed nitric acid as shown in Figure 5b. Due to this decrease, the values of the uptake coefficient reported

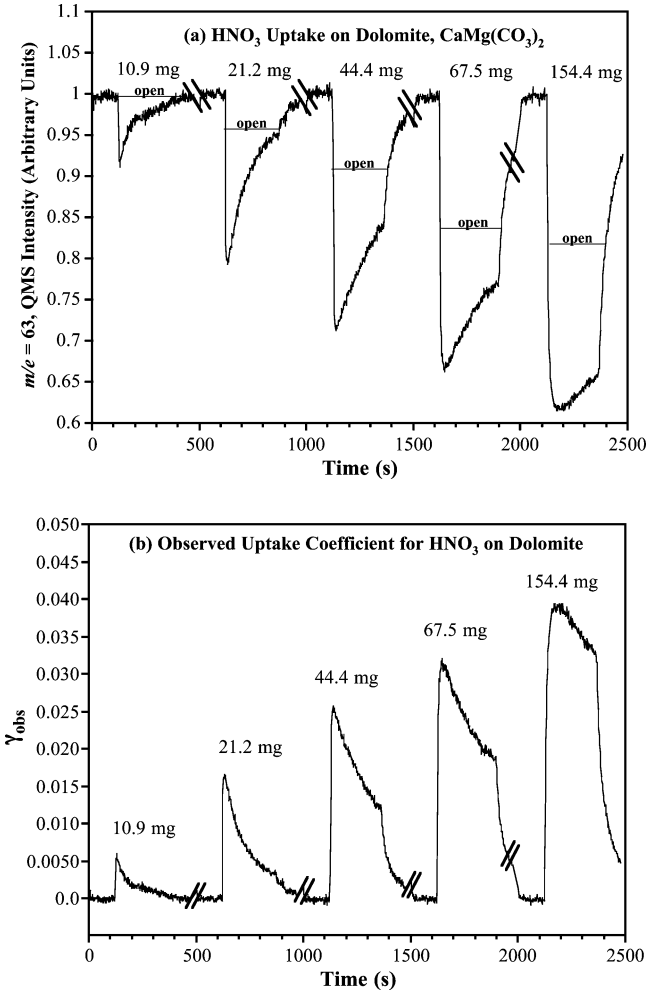

Figure 5. (a) QMS intensity ($m/e = 63$) plotted as a function of time for HNO_3 uptake on dolomite powder (BET surface area of 0.6 m^2 g^{-1}). "Open" refers to the time the sample holder is open is and the particles are exposed to nitric acid vapor. (b) Calculated observed uptake coefficient using eq 2 with $A_h = 0.324$ cm^2 and $A_s = 5.07$ cm^2. The results of several different experiments are shown. The data have been displaced in time with respect to each other.

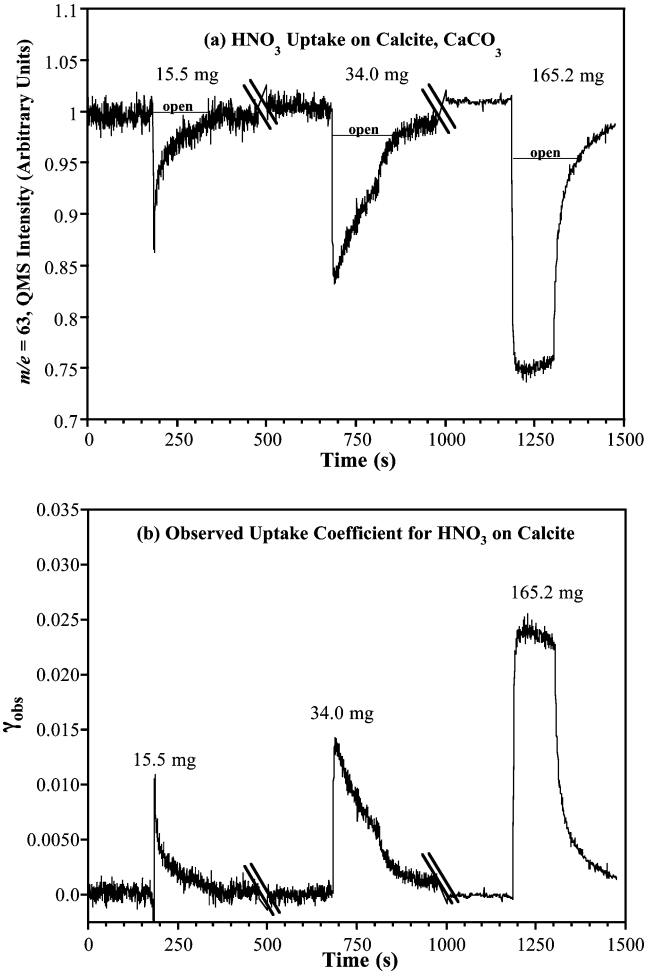

Figure 6. (a) QMS intensity ($m/e = 63$) plotted as a function of time for HNO_3 uptake on calcite powder (BET surface area of 0.2 m^2 g^{-1}) of various mass. "Open" refers to the time the sample holder is open is and the particles are exposed to nitric acid vapor. (b) Calculated observed uptake coefficient using eq 2 with $A_h = 0.363$ cm^2 and $A_s = 5.34$ cm^2 for the data shown in (a). The results of three different experiments are shown. The data have been displaced in time with respect to each other.

here are the initial uptake coefficients and are taken as the maximum value of the uptake coefficient.

Similar results are obtained for the uptake of HNO_3 on calcite. Figure 6a shows the QMS intensity versus time data for HNO_3 on calcite. Several different masses are shown. The surface area of the calcite powder used is 0.2 m^2 g^{-1}. The observed uptake coefficient calculated using eq 2 is shown in Figure 6b. The initial value of the uptake coefficient increases as the mass increases. Although not shown, a similar trend is also observed for the 1.4 m^2 g^{-1} surface area calcite during experiments carried out using 1.9×10^{11} molecules cm^{-3} (6 μTorr) of HNO_3.

The standard Knudsen cell equation fails to account for mass dependent behavior that is observed in the uptake of HNO_3 on carbonate particles. This is because in its derivation, it is assumed that an approaching gas molecule collides once and only once with the top layer of the surface of the sample (whose area is assumed to be the geometric area) and does not diffuse into lower particle layers. However, the mass-dependent behavior that is observed can be accounted for through the use of gas diffusion models for these multiple particle layer experiments.

Pore Diffusion Model Adapted for Atmospherically Relevant Systems and Its Application to the Heterogeneous Uptake of HNO_3 on Multiple Layers of Carbonate Particles. Keyser, Moore, and Leu adapted a model from heterogeneous catalysis literature to take into account diffusion into underlying layers of a porous sample in heterogeneous atmospheric reactions.[33] The details of this model are summarized elsewhere and will not be presented here. The model includes two contributions to the uptake coefficient, one from external (surface) and one from internal (underlying layers) particle surface area. These contributions are related to γ_{obs} by

$$\gamma_{obs} = \gamma_t\left(\frac{S_e + \eta S_i}{A_s}\right) \tag{3}$$

where

$$\eta = \frac{1}{\phi}\tanh(\phi) \tag{4}$$

and

$$\phi = \frac{m}{\rho_b A_s d}\left(\frac{3\rho_b}{\rho_t - \rho_b}\right)\left(\frac{3\tau\gamma_t}{4}\right)^{1/2} \tag{5}$$

The term in parentheses in eq 3 is a correction to account for diffusion into underlying layers. S_e and S_i are the external and

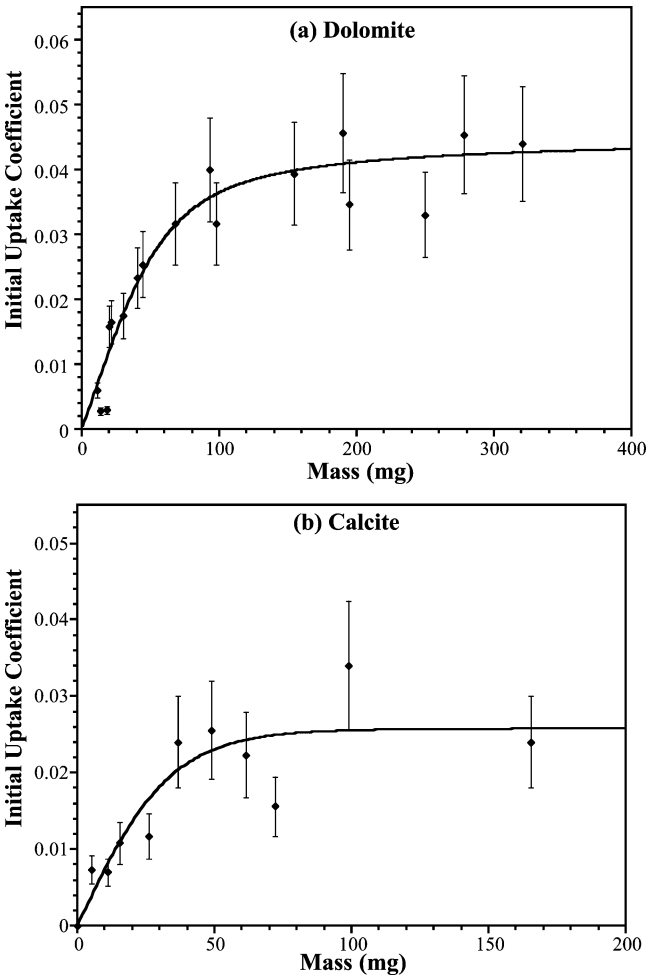

Figure 7. Initial uptake coefficients calculated using eq 2 are plotted as a function of sample mass for (a) HNO_3 uptake on dolomite, $CaMg(CO_3)_2$ (0.64 $m^2\ g^{-1}$), at a HNO_3 concentration of 6.5×10^{10} molecules cm^3 and (b) HNO_3 uptake on calcite, $CaCO_3$ (0.2 $m^2\ g^{-1}$), at a HNO_3 concentration of 6.5×10^{10} molecules cm^3. The line through the data are fit to the data using eqs 3−6 and the parameters given in Table 1.

internal surface areas, respectively, and η is an "effectiveness factor" that represents the fraction of the internal area that contributes to the measured uptake coefficient. The effectiveness factor is mass dependent and determined from the relative rates of surface adsorption and diffusion into underlying layer. The tortuosity constant, τ, corrects for inhomogenities in the interparticle voids and typically has a value in the range of 1−8 but must be experimentally determined for most porous solids. Also entering into the calculation of η are the mass, m, the bulk density, ρ_b, the true density, ρ_t, and the particle diameter, d. Rewriting eq 3 in terms of BET surface area (S_{BET}) and measured bulk density yields

$$\gamma_{obs} = \gamma_t \rho_b S_{BET}(h_e + \eta h_i) \qquad (6)$$

where h_e is the height of the first layer and h_i is the height of all the internal layers.

Figure 7 shows the measured initial uptake coefficient for HNO_3 on (a) dolomite and (b) calcite as a function of the sample mass. For dolomite, the value of γ_{obs} increases with sample mass to approximately 70 mg, after which it begins to plateau and reach a constant value independent of mass. In this plateau region, the initial uptake coefficient is ~0.04. The observed initial uptake coefficient is dependent on the thickness of the sample and thus the number of particle layers present in the sample. Using the KML model, fits were obtained for the initial uptake coefficient versus sample mass data presented for dolomite and calcite and are presented in Figure 7. The parameters used for the fits are given in Table 1. The best fit result of the KML model for HNO_3 uptake on dolomite was given by using $\tau = 7.0$ and $\gamma_t = (5 \pm 2) \times 10^{-4}$. The model fits both the form and the measured values for dolomite fairly well. For calcite, fits were determined for the different surface area samples by using $\tau = 5.3$ and $\gamma_t = (2 \pm 1) \times 10^{-3}$ and $\tau = 2.7$ and $\gamma_t = (2 \pm 1) \times 10^{-3}$ for the 1.4 and 0.2 $m^2\ g^{-1}$ powders, respectively. Only the data collected for the calcite sample with a surface area of 0.2 $m^2\ g^{-1}$ are shown in Figure 7b. Again, the model fits the experimental data for both surface area powders fairly well.

Linear Mass-Dependent Regime (LMD) Model and Its Application to the Uptake of HNO_3 on Multiple Layers of Carbonate Particles. As sample mass increases, HNO_3 uptake increases as well for both carbonates, until a constant value is reached at higher masses. For smaller, thinner samples, the initial uptake coefficient is directly proportional to sample mass as HNO_3 molecules are able to diffuse through and access the entire sample. This region is entitled the linear mass-dependent (LMD) regime. The LMD model is used to determine the correction factor that is necessary and its derivation is described in detail elsewhere.[12] The result is a modification to eq 2, the standard Knudsen cell equation, where the geometric area of the sample holder has been replaced with the BET surface area of the powder sample.

$$\gamma_t = \frac{A_h}{A_{BET}}\left(\frac{I_0 - I}{I}\right) = \left(\frac{A_s}{A_{BET}}\right)\gamma_{obs} \qquad (7)$$

In this equation, γ_t is the true initial uptake coefficient and A_{BET} is the BET area of the entire sample. Using eq 7, γ_t can be calculated from the known mass and observed uptake coefficient for individual experiments. To reduce random error, γ_t can also be determined using the slope of the best linear fit to the initial uptake coefficient versus mass data through

$$\gamma_t = \text{slope } (mg^{-1})\left(\frac{A_s\ (cm^2)}{S_{BET}\ (cm^2\ mg^{-1})}\right) \qquad (8)$$

Using eq 8 and the data shown in Figure 7 for the smaller masses in the linear regime, initial uptake coefficients for the two

TABLE 1: Parameters Used To Model HNO_3 Uptake on Multiple Layers of $CaMg(CO_3)_2$ and $CaCO_3$ Particles

parameter	symbol	$CaMg(CO_3)_2$	$CaCO_3$	$CaCO_3$
diameter	d	53 μm	5 μm	3 μm
specific surface area	S_{BET}	0.6 $m^2\ g^{-1}$	0.2 $m^2\ g^{-1}$	1.4 $m^2\ g^{-1}$
true density	ρ_t	2.9 g cm^{-3}	2.9 g cm^{-3}	2.9 g cm^{-3}
bulk density	ρ_b	2.6 g cm^{-3}	0.5 g cm^{-3}	0.8 g cm^{-3}
true uptake coefficient	γ_t	$(5 \pm 2) \times 10^{-4}$	$(2 \pm 1) \times 10^{-3}$	$(2 \pm 1) \times 10^{-3}$
tortuosity factor	τ	7.0	2.7	5.3
HNO_3 pressure	P	2 μTorr	2 μTorr	6 μTorr
HNO_3 concentration	n/V	6.5×10^{10} molecules/cm^3	6.5×10^{10} molecules/cm^3	1.9×10^{11} molecules/cm^3

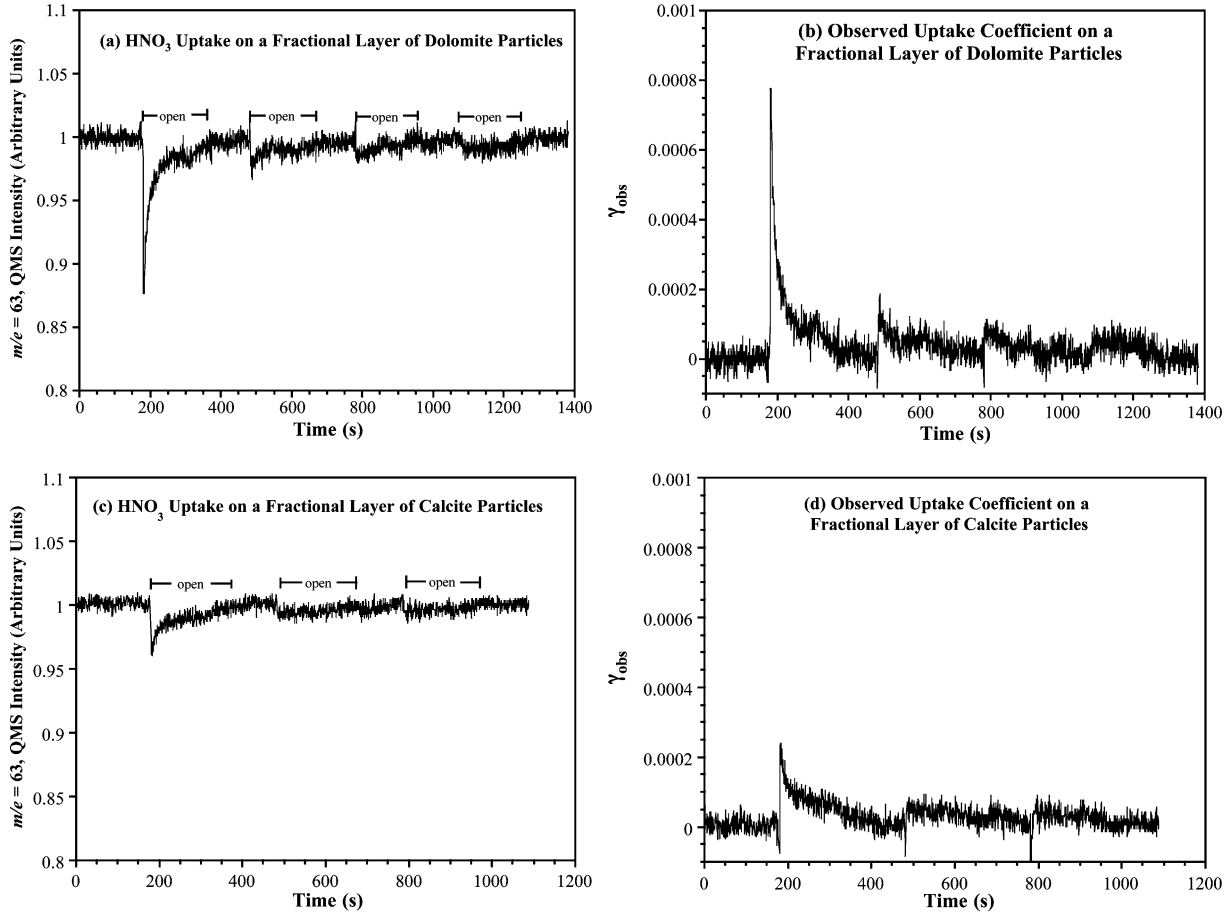

Figure 8. (a) QMS intensity ($m/e = 63$) plotted as a function of time for HNO_3 uptake on a fractional layer of dolomite particles (27.3 mg of $CaMg(CO_3)_2$) (b) Calculated observed uptake coefficient using eq 2 with $A_h = 0.324$ cm^2 and $A_s = 58.5$ cm^2 for the data shown in (a). (c) QMS intensity ($m/e = 63$) plotted as a function of time for HNO_3 uptake on a fractional layer of calcite particles (9.4 mg of $CaCO_3$, surface area of 1.4 m^2 g^{-1}) (b) Calculated observed uptake coefficients using eq 2 with $A_h = 0.324$ cm^2 and $A_s = 58.5$ cm^2 for the data shown in (c).

carbonates were determined to be $(4 \pm 2) \times 10^{-4}$ for dolomite and $(2 \pm 1) \times 10^{-3}$ for calcite. These values are in good agreement with those determined using the pore diffusion model discussed above.

Knudsen Cell Reactor Results for Samples Containing a Fractional Particle Layers. A new approach to determining the surface area available in a sample made up of particles was recently proposed and described in detail by Hoffman et al.[30] The method employs the use of fractional layers of particle to calculate surface area and determine a true uptake coefficient for the reaction of gaseous HNO_3 on NaCl. Diffusion problems that arise with multilayer samples are eliminated through the use of fractional particle layers; however, as discussed below, the available reactive surface area must still be determined.

Experiments using fractional particle layers were carried out for both types of carbonates. For calcite, experiments using fractional particle layers were conducted using particles with a surface area of 1.4 m^2 g^{-1}. Representative Knudsen cell data are displayed in Figure 8 for both dolomite and calcite. The HNO_3 concentration was 6.5×10^{10} molecules cm^{-3} in these experiments corresponding to a pressure of 2 μTorr. In Figure 8, the QMS data are shown as well as the calculated observed uptake coefficient using eq 2.

A true initial uptake coefficient can be calculated for the samples consisting of less than one fractional particle layer. If the BET surface area is used as the available surface area, then a value of $(1.0 \pm 0.3) \times 10^{-4}$ is obtained for calcite. For the dolomite samples, an initial uptake coefficient of $(2 \pm 1) \times 10^{-4}$ is obtained. Both of these values are significantly lower than what is obtained from the experiments on multiple layers of particles.

Hoffman et al. recently described another method for calculating the surface area that differs from the simple analysis using the BET surface area. The surface area available for reaction in this new method is dependent upon the area of the tops of the particles and a fraction of the area of the particle sides. The bottoms of the particles, i.e., the portion of the particles in direct contact with the sample holder, are considered to be unavailable for reaction. The area of the tops of the particles can be calculated using average particle dimensions, as determined by SEM. Calculating the available area of the sides is slightly more complicated. If an incoming HNO_3 gas molecule strikes the empty space of the sample holder rather than the top of a particle, it can potentially be scattered into the side of a particle. The portion of HNO_3 molecules that are capable of this is determined from the proximity of the particle to each other and the scattering angle, θ, which is calculated from

$$\theta = 90 - \arctan\frac{a}{b} \tag{9}$$

where a is the height of the carbonate particle and b is half the distance between two particles, assuming that an HNO_3 molecule strikes the sample holder surface equidistant from evenly spaced carbonate particles. By integrating over the 360° horizontal

TABLE 2: Summary of Results from Dolomite and Calcite Experiments Using Less Than One Fractional Particle Layer

mass (mg)	fractional particle layers	γ_{obs}	$\gamma_{o,t}$(BET)	$\gamma_{o,t}$(corrected)
		Dolomite		
18.6	0.26	2.3×10^{-4}	1.1×10^{-4}	3.5×10^{-4}
20.9	0.29	2.9×10^{-4}	1.3×10^{-4}	4.6×10^{-4}
26.0	0.37	6.3×10^{-4}	2.1×10^{-4}	9.7×10^{-4}
27.6	0.39	7.4×10^{-4}	2.5×10^{-4}	1.2×10^{-3}
av		$(5 \pm 3) \times 10^{-4}$	$(2 \pm 1) \times 10^{-4}$	$(7 \pm 4) \times 10^{-4}$
		Calcite		
4.3	0.08	1.5×10^{-4}	1.4×10^{-4}	1.7×10^{-3}
4.4	0.09	1.6×10^{-4}	1.5×10^{-4}	1.8×10^{-3}
9.4	0.18	2.4×10^{-4}	1.1×10^{-4}	1.3×10^{-3}
av		$(1.8 \pm 0.5) \times 10^{-4}$	$(1.3 \pm 0.2) \times 10^{-4}$	$(1.5 \pm 0.4) \times 10^{-3}$

plane, the fraction of molecules for which the scattering angle is $\geq \theta$ can be determined. This fraction (F) is given by the cosine law for molecular scattering.

$$F = \cos^2 \theta \tag{10}$$

Even if the scattering angle is large enough for a HNO_3 molecule to collide with the side of a particle, it may pass through open space between the particles instead. Because of this, F must be reduced to account for this open space using the average dimensions of the particles and the distance between them. The new fraction is denoted as F'. Using the area of the tops of the particles and F', the true reactive surface area can be calculated from

$$\text{true reactive area} = A_{top} + (A_s - A_{top})F' \tag{11}$$

where A_{top} is the total surface area for the tops of the particles. Using this model, Hoffman and co-workers were able to determine a corrected initial uptake coefficient for the uptake of HNO_3 on NaCl to be $(2.3 \pm 1.9) \times 10^{-3}$.

Using this model, we have been able to calculate a corrected initial uptake coefficient for HNO_3 on dolomite in these fractional layer experiments. The average particle diameter and spacing for dolomite submonolayer samples were both 5 μm. With this spacing and particle size, the corrected initial uptake coefficient has an average value of $(7 \pm 4) \times 10^{-4}$. Results from each individual submonolayer experiment for dolomite and calcite are given in Table 2. A corrected value of for HNO_3 uptake on calcite particles in these fractional layer experiments was also determined, using an average particle size of 3 μm and an average spacing of 37 μm. With these parameters, an average initial value of $(2.0 \pm 0.4) \times 10^{-3}$ for HNO_3 uptake on calcite was determined. By comparison of the values of the corrected initial uptake for both carbonates, it can be seen that these results are in good agreement with the experiments done on multiple particle layers and analyzed for internal surface area due to uptake on particles below the first layer. Uncertainty in the values of γ calculated using less than one layer of particles come from several sources, including particle size, shape, and spacing on the sample holder surface. For these calculations, the particles are assumed to be cubic and uniform in size, as well as evenly spaced on the sample holder.

Surface Saturation and Product Formation. Surface coverages were also determined in the Knudsen cell reactor experiments using fractional and single layers of particles by allowing the carbonate powder to completely react with the HNO_3. This is done by repeatedly exposing the sample to HNO_3 until uptake is no longer observed. The HNO_3 QMS intensity can be converted to the number of molecules lost to the surface per second as a function of time. The area under the resultant is integrated and a surface coverage determined. Representative data for determining saturation coverages of nitric acid on dolomite and calcite are shown in Figure 9. Analysis of five different experiments yields an average saturation surface coverage of $(1.1 \pm 0.9) \times 10^{14}$ molecules cm^{-2} for dolomite. For calcite, an average surface coverage of $(1.8 \pm 0.5) \times 10^{14}$ molecules cm^{-2} is determined on the 1.4 m^2 g^{-1} surface area sample and $(8 \pm 5) \times 10^{13}$ molecules cm^{-2} on the 0.2 m^2 g^{-1} sample.

Gas-phase H_2O and CO_2 are expected as products of the reaction between nitric acid and carbonates, as shown in reaction 1 for the calcite reaction. For dolomite samples greater than 20 mg, there is visible production of CO_2, observed by monitoring

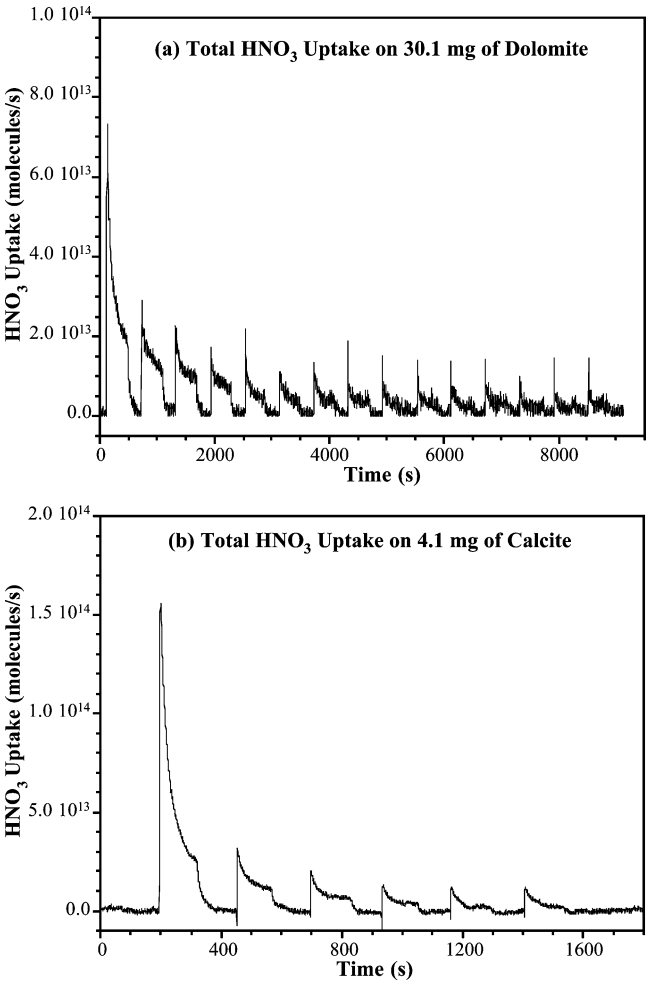

Figure 9. HNO_3 taken up on the surface (molecules s^{-1}) vs time data for (a) 30.1 mg dolomite, $CaMg(CO_3)_2$ (0.64 m^2 g^{-1}), sample and (b) 4.1 mg calcite, $CaCO_3$ (0.20 m^2 g^{-1}), sample. The integrated areas from these plots were used to calculate saturation coverages (molecules cm^{-2}) for HNO_3. The sample holder was opened and closed several times during the course of these measurements to check baseline drift.

an increase of the CO_2^+ ($m/e = 44$) QMS intensity while the powder sample is open and exposed to the HNO_3 gas. However, after calibrating the QMS intensities for the different gases, it was determined that the total number of CO_2 molecules produced by the reaction is less than 10% of the total number of HNO_3 molecules consumed under the dry conditions used in this study. There is also a visible increase in the $m/e = 44$ QMS intensity when calcite is exposed to HNO_3. An increase in the water signal is also observed, but only 20% of the amount expected on the basis of stoichiometry. This is evident from an increase in the $m/e = 18$ QMS signal during exposure. This result is consistent with the findings of other groups who have also observed the production of CO_2 and H_2O as products of reaction of nitric acid with calcite.[26,34,39] However, the amount of product is far less than expected on the basis of the bulk reaction. Reasons for this discrepancy are discussed in the next section.

Discussion

Reaction of Nitric Acid with Calcite and Dolomite under Dry Conditions. Equation 1 describes the bulk reaction between calcium carbonate and nitric acid. Experimental and theoretical surface science studies[40−45] have shown that the calcium carbonate surface is terminated by OH under ambient conditions, as a result of the dissociative adsorption of H_2O. These OH and CO_3H groups persist even in ultrahigh vacuum conditions.[46,47] The surface stoichiometry of calcite is best represented as $Ca(OH)(CO_3H)$. Under dry conditions, the surface reaction of HNO_3 with calcite results in the formation of adsorbed carbonic acid (H_2CO_3) according to reaction 12.

$$Ca(OH)(CO_3H) + HNO_3 \rightarrow Ca(OH)(NO_3) + H_2CO_3 \quad (12)$$

This reaction has been verified by FT-IR spectroscopy.[48,49] Once the particle surface saturates with a layer of adsorbed carbonic acid, uptake of nitric acid ceases. Thus carbonic acid blocks sites for further reaction. However, in the presence of adsorbed water, carbonic acid is unstable and dissociates into CO_2 and H_2O, allowing for further HNO_3 uptake. The minimal amount of gaseous CO_2 and H_2O detected as reaction products in the Knudsen cell experiment is an indication that there is adsorbed carbonic acid that remains on the calcite surface under the dry conditions used in these experiments. As noted above, to date there has been no spectroscopic study of the nitric acid reaction with the dolomite surface; however, the amount of CO_2 and H_2O detected in the gas phase in the Knudsen cell experiment is much less than what is expected from stoichiometry, suggesting that its surface chemistry resembles that of calcite.

Value of the Heterogeneous Uptake Coefficient of the Reaction of Nitric Acid with Calcite and Dolomite under Dry Conditions. One of the difficulties in using eq 2 to calculate heterogeneous uptake coefficients is that in its derivation it is assumed that there is continuous, steady-state uptake. This is not the case for adsorption on a finite number of surface sites. Instead, the uptake coefficient starts at a maximum value and then often begins to decrease as the sample surface becomes saturated. As discussed by Li et al.,[13] the observed uptake coefficient is therefore a lower limit to the true uptake coefficient because a finite number of surface sites prevent the steady-state uptake assumed in the derivation of eq 2 from being achieved. In this situation, when the uptake coefficient depends on surface coverage, the experimentally measured value becomes dependent on the residence time in the Knudsen cell reactor and thus the escape rate, k_{esc}, of gas-phase molecules out of the reactor as well as the gas pressure and the value of the uptake coefficient. In addition, for multilayer samples, it is important to consider both surface coverage and gas diffusion into the many layers of the powder sample during the time scale of the measurement.

In the heterogeneous uptake of HNO_3 on $CaCO_3$, surface saturation and gas diffusion through particle layers occur on the same time scale.[34] When these time scales are similar, there is a significant dependence on the parameters noted above. The escape constant, k_{esc}, itself depends on the reactor volume and the size of the escape aperture as shown in

$$k_{esc} = \frac{cA_h}{4V} \quad (13)$$

where c is the average molecular speed of the gas, A_h is the size of the aperture, and V is the volume of the reactor. Computer simulations[13] show that because the use of larger escape apertures and smaller volume results in larger values of k_{esc}, more accurate values of the uptake coefficient can be obtained as the response time of the system is faster. As k_{esc} increases, the experimental value increases as well and approaches the true value of what the initial uptake coefficient would be if there were no coverage effects.[13] In the current study a Knudsen cell reactor with a smaller volume and a larger aperture size, both of which should help eliminate saturation effects, have been used to determine the initial uptake coefficient. Thus, an increase in the value of γ for the calcite experiments reported here is observed from that previously reported.[28,34]

The shape of the data obtained with the Knudsen cell also changes when the hole or aperture size is changed. When a larger aperture is used, the response of the Knudsen cell reactor to changes in the gas concentrations inside it is faster.[13] The resulting QMS intensity versus time curve has a more well-defined minimum, leading to a more well-defined maximum when γ is plotted versus time. Li et al. also discuss the effect of pressure on the measured initial uptake coefficient; i.e., higher pressures will show larger saturation effects. The uptake coefficient previously reported by Goodman et al.[34] was measured at 40 μTorr, whereas experiments in the current study were conducted primarily at 2 μTorr. The decrease in pressure results in a higher measured value of γ_{obs}. The value of $\gamma_{o,t}$ for calcite reported here, $(2 \pm 1) \times 10^{-3}$, is a factor of about 8 times greater than the value of $(2.5 \pm 0.1) \times 10^{-4}$ previously reported.[34] This discrepancy is due to the different conditions used in the two studies, mainly differences in reactor volume and aperture size, and the pressure conditions during individual experiments. The data presented here also suggest that there are some saturation effects as well but less than those previously reported as the gas pressures (concentrations) used here are lower.

These new data for the uptake of HNO_3 on $CaCO_3$ are still lower than values reported by Hanisch et al.,[26] $(10 \pm 2.5) \times 10^{-2}$ at a similar HNO_3 concentration and Fenter et al.,[39] $(10 \pm 2) \times 10^{-2}$. Neither of these values has been corrected to account for internal surface area contributions. Hanisch et al. assume, on the basis of the results for HNO_3 uptake on other surfaces and from Fenter et al., that there is no mass dependence for the uptake of HNO_3 on $CaCO_3$ and no need for a correction to be made. The results presented in this work display a clear mass dependence and thus a need to correct γ_{obs} to account for internal surface area contributions.

The uptake coefficient for the heterogeneous uptake of HNO_3 on dolomite that we report as $(4 \pm 2) \times 10^{-4}$ is several orders

TABLE 3: Summary of Knudsen Cell Reactor Results for HNO_3 Uptake on $CaMg(CO_3)_2$ and $CaCO_3$

	$CaMg(CO_3)_2$ (0.6 m^2 g^{-1})	$CaCO_3$ (0.2 m^2 g^{-1})	$CaCO_3$ (1.4 m^2 g^{-1})
	Multilayer Samples		
γ_t(KML)	$(5 \pm 2) \times 10^{-4}$	$(2 \pm 1) \times 10^{-3}$	$(2 \pm 1) \times 10^{-3}$
saturation coverages (molecules cm^{-2})	$(1.1 \pm 0.9) \times 10^{14}$	$(8 \pm 5) \times 10^{13}$	$(1.8 \pm 0.5) \times 10^{14}$
	Fractional Layer Samples		
$\gamma_{o,t}$(BET)	$(2 \pm 1) \times 10^{-4}$		$(1 \pm 0.3) \times 10^{-4}$
$\gamma_{o,t}$ (corrected)	$(7 \pm 4) \times 10^{-4}$		$(8 \pm 2) \times 10^{-4}$

of magnitude lower than that reported by Hanisch et al.,[27] 14×10^{-2}. Although their study was the first to report a value of the uptake coefficient for HNO_3 on dolomite, it was limited to a single sample mass. No conclusion can be made about the mass dependence of γ_{obs} from that study.

Results obtained through the use of the fractional layer model proposed by Hoffman et al. yield a value of the calculated initial uptake coefficient for both dolomite and calcite that is consistent with that measured for multiple layers. Uncertainty in the values of γ calculated using less than one layer of particles come from several sources, including particle size, shape, and spacing on the sample holder surface. For these calculations, the particles are assumed to be cubic and uniform in size, as well as evenly spaced on the sample holder. Clearly, this is a crude approximation to the randomly spaced, irregularly shaped particles observed in SEM (see Figures 3 and 4).

The data presented here indicate that calcite is slightly more reactive than dolomite by a factor of 4. One possible explanation for this difference in reactivity can be attributed to the stability of the calcite and dolomite surfaces relative to each other. A recent theoretical study examined the stabilities of the $CaCO_3$, $CaMg(CO_3)_2$, and $MgCO_3$ $(10\bar{1}4)$ surfaces under dry and hydrated conditions,[50] it was found that in both cases, the calcite surface was the least stable, making it more likely to undergo reaction. The dolomite surface was the most stable under dry conditions. A complete summary of all Knudsen cell results for these experiments can be found in Table 3. The results presented here provide improved measurements of γ_{HNO_3} on dolomite and calcite under dry conditions. The agreement of different analysis methods used to account for internal surface area indicates that these contributions must be considered in order to accurately determine the heterogeneous uptake coefficient for these reactions.

Recommendations for Future Laboratory Studies and Modeling Analysis To Better Assess the Impact of Heterogeneous Reaction of Nitric Acid on Carbonate-Containing Mineral Dust Aerosol and Conclusions

In analyzing the impact of dust on tropospheric ozone, Bian and Zender[8,51] state that the irreversible uptake of HNO_3 is the most important and the most uncertain parameter in their study. Results of a box-model study have shown that values the uptake coefficient for nitric acid greater than 10^{-5} represented a loss mechanism for nitric acid in the atmosphere.[28] The loss of HNO_3 leads to a decrease in the predicted HNO_3 concentration and the HNO_3 to NO_x ratios. Because the experiments described here were conducted under dry conditions, they represent a lower limit for the heterogeneous uptake coefficient. Near 0% relative humidity, the carbonate surface will become saturated over time, thus preventing further uptake of HNO_3. This surface passivation is not an issue at higher relative humdities, as it has been shown in other studies from our laboratory that the presence of adsorbed water can enhance the extent of reaction as the nitrate product that forms deliquesces at relative humidities near 10%.[52−54] Nitric acid can diffuse through this deliquescent layer and further react with $CaCO_3$. In addition, other laboratory experiments from our laboratory have shown that nitric acid kinetics can be enhanced in the presence of adsorbed water. Therefore, under conditions more representative of the atmosphere, 20−90% relative humidity, the uptake of nitric acid may increase by as much as a factor of 10−50.[29,55,56] The two carbonates investigated here would then have initial uptake coefficients in the range of 0.001 to 0.1 under atmospherically relevant conditions and reactions with these carbonates is expected to be a loss mechanism for nitric acid.

Results obtained through modeling analysis are often sensitive to the values of uptake coefficients selected, which are taken to be globally uniform despite the variations in dust composition from different sources.[15,57] However it is important to note that different components of mineral dust, e.g., calcite, quartz, clays, and gypsum, react very differently with nitric acid.[26,27,29,34,35,54,58] Currently, the "state-of-the-art" in modeling analysis is that mineral dust aerosol is treated as a single entity aerosol and is often just represented as a size distribution, failing to account for variations in its chemical composition. These differences in reactivity of the different components must be included in models to accurately predict the effect mineral dust aerosol has on atmospheric processes. The reactivity of a mineral dust particle may also change over time as the particle ages in the atmosphere and very little is known about how particle aging effects reactivity.

Though Bian and Zender note the uncertainty of γ_{HNO_3} in their study, they use only a single value for γ_{HNO_3} and fail to account for particle mineralogy in their simulations, although they do recognize the need to include it if a reliable prediction of the effects of mineral dust on tropospheric processes is to be made.[51] Therefore better model representations of global dust composition and the effects of relative humidity and aging should be included in atmospheric chemistry models.

To further reduce uncertainty in model results and because modeling studies depend on results from laboratory experiments, further work is needed to improve measurements for γ_{HNO_3} on mineral dust components and to further reconcile the disparity between reported values of γ_{HNO_3} are required. Recommendations for future laboratory experiments include:

- measure reaction kinetics of nitric acid on the components of mineral dust aerosol at higher relative humidities;
- measure reaction kinetics of of nitric acid on the components of mineral dust aerosol in complex mixtures of gases that better represent the gas-phase chemical composition of polluted environments;
- measure reaction kinetics of complex mixtures of authentic mineral dust aerosol using single particle techniques to better distinguish differences in dust reactivity.

Acknowledgment. We gratefully acknowledge support from the National Science Foundation through a creativity extension of grant CHE-9984344 and CHE-.

References and Notes

(1) Jonas, P. R.; Charlson, R. J.; Rodhe, H. Aerosols. In *Climate Change 1994: Radiative Forcing of Climate Change and an Evaluation of the IPCC 1992 IS92 Emission Scenarios*; Houghton, J. T., Meira Filho, L. G., Bruce, J. P., Lee, H., Callander, B. A., Haites, E. F., Eds.; Cambridge University Press: New York, 1995.

(2) Li, X.; Maring, H.; Savoie, D.; Voss, K.; Prospero, J. M. *Nature* **1996**, *380*, 416.

(3) Prospero, J. M. *Proc. Natl. Acad. Sci. U.S.A.* **1999**, *96*, 3396.

(4) Gomes, L.; Gillette, D. A. *Atmos. Environ., Part A* **1993**, *27A*, 2539.

(5) Dentener, F. J.; Carmichael, G. R.; Zhang, Y.; Lelieveld, J.; Crutzen, P. J. *J. Geophys. Res.* **1996**, *101*, 22869.

(6) Bauer, S. E.; Balkanski, Y.; Schulz, M.; Hauglustaine, D. A.; Dentener, F. J. *J. Geophys. Res.* **2004**, *109*, D02304, doi: 10.1029/2003JD003868.

(7) Martin, R. V.; Jacob, D. J.; Yantosca, R. M.; Chin, M.; Ginoux, P. *J. Geophys. Res.* **2003**, *108*(D3), 4097, doi: 10.1029/2002JD002622.

(8) Bian, H.; Zender, C. S. *J. Geophys. Res.* **2003**, *108*(D21), 4672, doi: 10.1029/2002JD003143.

(9) Tang, Y.; Carmichael, G. R.; Kurata, G.; Uno, I.; Weber, R. J.; Song, C.-H.; Guttikunda, S. K.; Woo, J.-H.; Streets, D. G.; Wei, C.; Clarke, A. D.; Huebert, B.; Anderson, T. L. *J. Geophys. Res.* **2004**, *109*, D19S21, doi: 10.1029/2003JD003806.

(10) Song, C. H.; Carmichael, G. R. *J. Atmos. Chem.* **2001**, *40*, 1.

(11) Tabazadeh, A.; Jacobson, M. Z.; Singh, H. B.; Toon, O. B.; Lin, J. S.; Chatfield, R. B.; Thakur, A. N.; Talbot, R. W.; Dibb, J. E. *Geophys. Res. Lett.* **1998**, *25*, 4185.

(12) Underwood, G. M.; Li, P.; Usher, C. R.; Grassian, V. H. *J. Phys. Chem. A* **2000**, *104*, 819.

(13) Li, P.; Al-Abadleh, H. A.; Grassian, V. H. *J. Phys. Chem. A* **2002**, *106*, 1210.

(14) Usher, C. R.; Michel, A. E.; Stec, D.; Grassian, V. H. *Atmos. Environ.* **2003**, *37*, 5337.

(15) Michel, A. E.; Usher, C. R.; Grassian, V. H. *Geophys. Res. Lett.* **2002**, *29*(14), 1665, doi: 10.1029/2002GL014896.

(16) Michel, A. E.; Usher, C. R.; Grassian, V. H. *Atmos. Environ.* **2003**, *37*, 3201.

(17) Hanisch, F.; Crowley, J. N. *Atmos. Chem. Phys.* **2003**, *3*, 119.

(18) Sullivan, R. C.; Thornberry, T.; Abbatt, J. P. D. *Atmos. Chem. Phys.* **2004**, *4*, 1301.

(19) Hoffman, R. C.; Gebel, M. E.; Fox, B. S.; Finlayson-Pitts, B. J. *Phys. Chem. Chem. Phys.* **2003**, *5*, 1780.

(20) Fenter, F. F.; Caloz, F.; Rossi, M. J. *J. Phys. Chem.* **1996**, *100*, 1008.

(21) Leu, M.-T.; Timonen, R. S.; Keyser, L. F.; Yung, Y. L. *J. Phys. Chem.* **1995**, *99*, 13203.

(22) Koch, T. G.; Van den Bergh, H.; Rossi, M. J. *Phys. Chem. Chem. Phys.* **1999**, *1*, 2687.

(23) Stewart, D. J.; Griffiths, P. T.; Cox, R. A. *Atmos. Chem. Phys.* **2004**, *4*, 1381.

(24) Fenter, F. F.; Caloz, F.; Rossi, M. J. *J. Phys. Chem.* **1994**, *98*, 9801.

(25) Beichert, P.; Finlayson-Pitts, B. J. *J. Phys. Chem.* **1996**, *100*, 15218.

(26) Hanisch, F.; Crowley, J. N. *J. Phys. Chem. A* **2001**, *105*, 3096.

(27) Hanisch, F.; Crowley, J. N. *Phys. Chem. Chem. Phys.* **2001**, *3*, 2474.

(28) Underwood, G. M.; Song, C. H.; Phadnis, M.; Carmichael, G. R.; Grassian, V. H. *J. Geophys. Res.* **2001**, *106*, 18055.

(29) Underwood, G. M.; Li, P.; Al-Abadleh, H.; Grassian, V. H. *J. Phys. Chem. A* **2001**, *105*, 6609.

(30) Hoffman, R. C.; Kaleuati, M. A.; Finlayson-Pitts, B. J. *J. Phys. Chem. A* **2003**, *107*, 7818.

(31) Zangmeister, C. D.; Pemberton, J. E. *J. Phys. Chem. A* **2004**, *108*, 236.

(32) Zangmeister, C. D.; Pemberton, J. E. *J. Phys. Chem. A* **2001**, *105*, 3788.

(33) Keyser, L. F.; Moore, S. B.; Leu, M. T. *J. Phys. Chem.* **1991**, *95*, 5496.

(34) Goodman, A. L.; Underwood, G. M.; Grassian, V. H. *J. Geophys. Res.* **2000**, *105*, 29053.

(35) Frinak, E. K.; Wermeille, S. J.; Mashburn, C. D.; Tolbert, M. A.; Pursell, C. J. *J. Phys. Chem. A* **2004**, *108*, 1560.

(36) Krueger, B. J.; Grassian, V. H.; Iedema, M. J.; Cowin, J. P.; Laskin, A. *Anal. Chem.* **2003**, *75*, 5170.

(37) Carlos-Cuellar, S.; Li, P.; Christensen, A. P.; Krueger, B. J.; Burrichter, C.; Grassian, V. H. *J. Phys. Chem. A* **2003**, *107*, 4250.

(38) Golden, D. M.; Spokes, G. N.; Benson, S. W. *Angew. Chem., Int. Ed. Engl.* **1973**, *12*, 534.

(39) Fenter, F. F.; Caloz, F.; Rossi, M. J. *Atmos. Environ.* **1995**, *29*, 3365.

(40) Stipp, S. L. S.; Gutmannsbauer, W.; Lehmann, T. *Am. Miner.* **1996**, *81*, 1.

(41) Kuriyavar, S. I.; Vetrivel, R.; Hegde, S. G.; Ramaswamy, A. V.; Chakrabarty, D.; Mahapatra, S. *J. Mater. Chem.* **2000**, *10*, 1835.

(42) de Leeuw, N. H.; Parker, S. C. *J. Phys. Chem. B* **1998**, *102*, 2914.

(43) Stipp, S. L. S.; Eggleston, C. M.; Nielsen, B. S. *Geochim. Cosmochim. Acta* **1994**, *58*, 2023.

(44) McCoy, J. M.; La Femina, J. P. *Surf. Sci.* **1997**, *373*, 288.

(45) Stoeckelmann, E.; Hentschke, R. *Langmuir* **1999**, *15*, 5141.

(46) Stipp, S. L.; Hochella, M. F., Jr. *Geochim. Cosmochim. Acta* **1991**, *55*, 1723.

(47) Stipp, S. L. S. *Geochim. Cosmochim. Acta* **1999**, *63*, 3121.

(48) Al-Hosney, H. A.; Grassian, V. H. *J. Am. Chem. Soc.* **2004**, *126*, 8068.

(49) Al-Hosney, H. A.; Grassian, V. H. *Phys. Chem. Chem. Phys.* **2005**, *7*, 1266.

(50) Wright, K.; Cygan, R. T.; Slater, B. *Phys. Chem. Chem. Phys.* **2001**, *3*, 839.

(51) Bian, H.; Zender, C. S. *J. Geophys. Res.*, submitted for publication.

(52) Al-Abadleh, H. A.; Krueger, B. J.; Ross, J. L.; Grassian, V. H. *Chem. Commun.* **2003**, 2796−2797.

(53) Krueger, B. J.; Grassian, V. H.; Laskin, A.; Cowin, J. P. *Geophys. Res. Lett.* **2003**, *30*(3), 1148, doi: 10.1029/2002GL016563.

(54) Laskin, A.; Wietsma, T. W.; Krueger, B. J.; Grassian, V. H. *J. Geophys. Res.* **2005**, *110*, D10208, doi: 10.1029/2004/JD005206.

(55) Goodman, A. L.; Bernard, E. T.; Grassian, V. H. *J. Phys. Chem. A* **2001**, *105*, 6443.

(56) Maxwell-Meier, K.; Weber, R.; Song, C.; Orsini, D.; Ma, Y.; Carmichael, G. R.; Streets, D. G. *J. Geophys. Res.* **2004**, *109*, D19S07, doi: 10.1029/2003JD004464.

(57) Sokolik, I. N.; Winker, D. M.; Bergametti, G.; Gillette, D. A.; Carmichael, G.; Kaufman, Y. J.; Gomes, L.; Schuetz, L.; Penner, J. E. *J. Geophys. Res.* **2001**, *106*, 18015.

(58) Krueger, B. J.; Grassian, V. H.; Laskin, A. J. Cowin *Atmos. Environ.* **2004**, *38*, 6253−6261.